Optics Letters

Dynamic control of spontaneous emission rate using tunable hyperbolic metamaterials

Sandeep Kumar Chamoli,[1,2] Mohamed ElKabbash,[3,4] Jihua Zhang,[3] and Chunlei Guo[1,3,*]

[1]State Key Laboratory of Applied Optics, Changchun Institute of Optics, Fine Mechanics and Physics, Chinese Academy of Sciences, Changchun 130033, China
[2]University of Chinese Academy of Science, Beijing 100039, China
[3]The Institute of Optics, University of Rochester, Rochester, New York 14627, USA
[4]e-mail: melkabba@ur.rochester.edu
*Corresponding author: guo@optics.rochester.edu

Received 12 December 2019; revised 13 February 2020; accepted 14 February 2020; posted 14 February 2020 (Doc. ID 385844); published 17 March 2020

We numerically investigate the dynamic control over the spontaneous emission rate of quantum emitters using tunable hyperbolic metamaterials (HMMs). The dispersion of a metal–dielectric thin-film stack at a given frequency can undergo a topological transition from an elliptical to a hyperbolic dispersion by incorporating a tunable metal or dielectric film in the HMM. This transition modifies the local density of optical states of the emitter and, hence, its emission rate. In the visible range, we use an HMM consisting of TiN and Sb_2S_3 and show considerable tunability in the Purcell enhancement and quantum efficiency as Sb_2S_3 phase changes from amorphous to crystalline. Similarly, we show tunable Purcell enhancement in the telecommunication wavelength range using a TiN/VO_2- HMM. Finally, tunable spontaneous emission rate in the mid-IR range is obtained using a graphene/MgF_2 HMM by modifying the graphene conductivity through changing its chemical potential. We show that using a metal nitride (for the visible and NIR HMMs) and a fluoride (for the mid-IR HMM) is important to get an appreciable change in the effective permittivity of the thin-film multilayer stack.

https://doi.org/10.1364/OL.385844

The spontaneous emission (SE) of a quantum emitter was thought to be an inherent property of luminescent materials. Proper understanding of SE, provided by Weisskopf and Wigner, showed that SE arises from the interaction between an emitter and its local electromagnetic field. According to Fermi's golden rule, the SE rate of an emitter is proportional to the number of propagating or evanescent electromagnetic modes available to the emitter to radiate into, i.e., its local density of optical state (LDOS) [1]. By modifying the electromagnetic environment of an emitter, it is possible to enhance or suppress its SE rate [2]. The Purcell factor determines the change in SE rate and is given by Γ_g/Γ_0, where Γ_g is the modified SE rate and Γ_0 is the SE rate in free space for an emitter [3]. However, once an emitter is placed in a given electromagnetic environment, its SE rate is fixed. The ability to actively modulate the SE rate has been shown recently by modulating the emitter's LDOS. The dynamic control over the SE rate opens new avenues for the generation of nonclassical light states [4], and can be used as the basis of a SE rate-based optical modulator [5]. Recent works dynamically controlled the SE rate of fluorescence at cryogenic temperatures by "molding" the radiation field in real time [4] or by modifying the exciton–cavity coupling strength [6]. The emission rate of phosphorescence was also modified in real time by modifying the local field felt by erbium atoms placed at a quarter-wave distance away from a phase-change material. A different route for real-time modulation of SE rate relies on plasmon-induced cooperative effects [5,7,8] where multiple emitters transfer their energy cooperatively to a metallic nano-antenna such that the emission rate is proportional to the number of excited emitters. The SE rate can be also controlled by modifying the LDOS at time scales longer than the emission rate, which enables the control over emission intensity without changing the excitation intensity [9] and can be used as an SE rate-based optical modulator with lower modulation rates. This was realized by field-effect optical permittivity modulation of ultrathin TiN film (for emission in the visible range) [9] and graphene sheet (for emission in the NIR range) [10]. However, the demonstrated SE rate modulation methods either rely on complex nanophotonic structures that require complex nanolithography, operate at cryogenic temperatures, or offer limited SE rate tunability.

An important class of materials with high LDOS are hyperbolic metamaterials (HMMs). HMMs are a class of metamaterials with a hyperbolic isofrequency curve ((k_x, k_y, k_z)). The LDOS in k-space corresponds to the volume between isofrequency contours at $\omega(k)$ and $\omega(k) + \Delta\omega$. For an emitter in free space, the LDOS corresponds to a thin spherical shell in k-space. However, for an HMM, the hyperbolic isofrequency contour is unbound, and a hyperboloidal shell has an infinite volume [1]. This means that the Purcell factor of an ideal HMM diverges for all wavelengths where the material enjoys hyperbolic

dispersion. In reality, the increase of the SE rate of emitters interacting with an HMM is due to the excitation of high-k modes as infinite-k modes are unrealistic. Accordingly, HMMs provide a broadband method to enhance the SE rate of emitters as opposed to photonic crystals and plasmonic nanocavities [1,2]. There are two types of HMMs: Type I where the uniaxial anisotropic permittivity values are such that $\varepsilon_{\parallel} = \varepsilon_x = \varepsilon_y > 0$ and $\varepsilon_{\perp} = \varepsilon_z < 0$, and Type II where the uniaxial anisotropic permittivity values are such that $\varepsilon_{\parallel} = \varepsilon_x = \varepsilon_y < 0$ and $\varepsilon_{\perp} = \varepsilon_z > 0$. $\varepsilon_{\parallel}$ and $\varepsilon_{\perp}$ are the parallel and perpendicular effective permittivity, respectively, and ε_x, ε_y, and ε_z are the effective permittivity in the x, y, and z directions, respectively. The frequency range, at which $\varepsilon_{\parallel}\varepsilon_{\perp} < 0$, corresponds to a hyperbolic dispersion region. Type II HMMs are usually realized using thin-film stacks consisting of alternating metal–dielectric bilayers. Using materials with tunable permittivity, thus, can tune HMM dispersion [11] as was shown in graphene-based HMMs [12,13], liquid-crystal-based HMMs [14], and phase-change material-based HMMs [15,16]. The multilayer effective permittivity can be conveniently calculated using the effective medium theory. The perpendicular and parallel permittivity of the system are given by [1]

$$\varepsilon_{\parallel} = f_m \varepsilon_m + f_d \varepsilon_d, \tag{1}$$

$$\varepsilon_{\perp} = \frac{\varepsilon_m \varepsilon_d}{f_m \varepsilon_m + f_d \varepsilon_d}, \tag{2}$$

where ε_d and ε_m are the complex permittivity of the metal and dielectric films, respectively, and f_m and f_d are the fill fraction of metal and dielectric films, respectively, and they can be calculated as follows: $f_{m=} f_m = \frac{t_m}{t_m + t_d}$ and $f_d = 1 - f_m$, where t_m and t_d are the layer thicknesses of metal and dielectric in a unit cell.

In this work, we propose to use tunable HMMs as a direct, broadband, and lithography free method to control the SE rate and emission intensity at room temperature. We show that by modifying the effective permittivity of a single component of a tunable HMM, the emitters' ability to excite high-k modes can be controlled as shown schematically in Fig. 1, particularly when the HMM undergoes a topological transition from elliptical to hyperbolic dispersion. We investigate three designs of actively tunable HMMs to modulate the SE rate over the visible, near-infrared (NIR), and mid-IR wavelength ranges. We also investigate the tunable quantum efficiency of emitters coupled to an active HMM in the visible range. Accordingly, the proposed method can control the SE rate and emission intensity for modulators and display applications.

Sb_2S_3 is a phase-change material that can undergo a reversible transition from a crystalline to an amorphous phase heating Sb_2S_3 to temperatures higher than 573 K (Cry phase) and $\sim$ 801 K (Amp phase) [17]. It possesses many attractive properties, namely, nanosecond switching speed, a large bandgap, and large contrast between the two phases in the visible range. Moreover, the large bandgap of Sb_2S_3 makes it ideal for applications in the visible range as it enjoys relatively low losses [18]. Figure 2 shows the refractive index and the extinction coefficient components of Sb_2S_3's complex refractive index [17]. The crystalline (Cry) phase of Sb_2S_3 enjoys a higher refractive index than amorphous (Amp) phase reaching a maximum difference of $\Delta n \sim 1$ at 614 nm. On the other hand, the extension

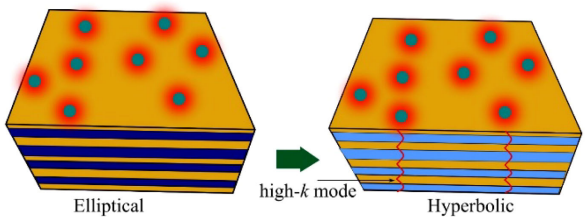

Fig. 1. Schematic of the system under study. Quantum emitters are situated at a distance $d \sim 10$ nm away from a multilayer thin-film stack consisting of metal–dielectric bilayers. One of the bilayers is an active material that can undergo a change in its optical properties. The change in the active layer optical property induces a topological transition of the multilayer effective permittivity, which transitions from elliptical to hyperbolic dispersion.

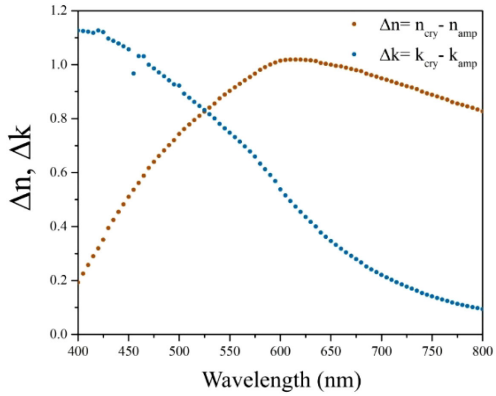

Fig. 2. Difference in the real and imaginary components of the complex refractive index of Sb_2S_3 between the crystalline (Cry) and amorphous (Amp) phases.

coefficient is negligible for wavelengths $\lambda > 605$ nm for the Amp phase and $\lambda > 714$ nm for the Cry phase. Consequently, including Sb_2S_3 as the dielectric component in an HMM enables control over its effective permittivity. According to the effective medium theory, however, the influence of changing phase on the effective permittivity depends on the permittivity of the metallic component. We choose TiN as the metallic film material, which behaves as a metal ($\mathrm{Re}(\varepsilon) < 0$) for $\lambda > 510$ nm [19]. Importantly, the complex permittivity value of TiN is significantly lower than that of other plasmonic metals such as Ag, Au, and Al. The lower complex permittivity values of TiN allow for accentuating the effect of the phase change of Sb_2S_3 on the effective permittivity of the HMM.

We consider an HMM constructed from five bilayers of TiN and Sb_2S_3 films. The Purcell factor F is given by $F = P_r + P_{nr}/P_0$, where P_r and P_{nr} are the power dissipated radiatively or nonradiatively, respectively, and P_0 is the power emitted by the dipole in an infinite uniform medium. The external quantum efficiency is given by $P_{\mathrm{rad}}/(F P_0)$ [20]. Since our goal is to maximize the difference in the Purcell factor (ΔF), we calculated the $\Delta F = F_{\mathrm{Cry}} - F_{\mathrm{Amp}}$ at 614 nm as a function of the Sb_2S_3 and TiN film thicknesses as shown in Fig. 3(a). Maximum ΔF is obtained for a Sb_2S_3 thickness of 45 nm, and a TiN thickness of 5 nm. Figures 3(b) and 3(c) show the parallel and perpendicular effective permittivity for the TiN/Sb_2S_3 (Cry) HMM, and TiN/Sb_2S_3 (Amp) HMM,

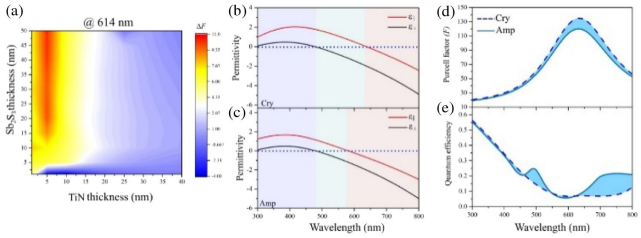

Fig. 3. Tunable spontaneous emission rate in the visible range: (a) calculated ΔF between TiN/Sb_2S_3 (Cry) HMM and TiN/Sb_2S_3 (Amp) HMM. The calculated effective parallel and perpendicular permittivity of (b) TiN/Sb_2S_3 (Cry) HMM and (c) TiN/Sb_2S_3 (Amp) HMM. The calculated (d) Purcell factor and (e) quantum efficiency for both HMMs.

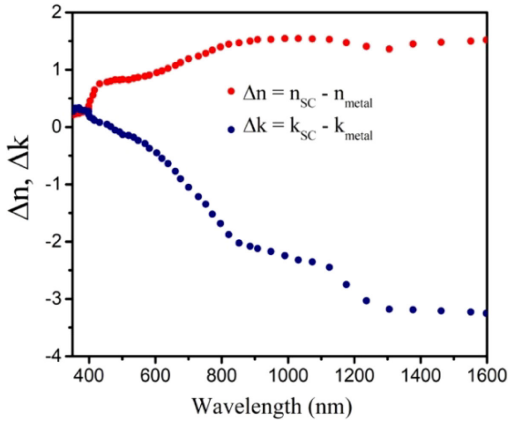

Fig. 4. Difference in the real and imaginary components of the complex refractive index of VO_2 between the semiconductor (SC) and metal phases.

respectively. While a topological transition to a type-I hyperbolic dispersion occurs for both HMMs at ~ 480 nm, the hyperbolic region extends to ~ 640 nm and 580 nm for the TiN/Sb_2S_3 (Cry) HMM and TiN/Sb_2S_3 (Amp) HMM, respectively. The calculated F for the two HMMs is shown in Fig. 3(d), demonstrating a significant increase in F for the TiN/Sb_2S_3 (Cry) HMM over a wide range of wavelengths reaching a maximum of $\Delta F = 15$ at ~ 630 nm. Figure 3(e) shows the calculated quantum efficiency for both HMMs. We note first that since the excited high-k modes are not coupled to the far field, the emission is quenched, leading to lower quantum efficiency. However, the quantum efficiency significantly differs between the two HMMs, which can be used for modulating the emission intensity without changing the excitation intensity [9]. If desired, patterning the HMM can outcouple the high-k modes, which can increase the quantum efficiency [20].

Vanadium dioxide (VO_2) is a promising material for optically active devices. It exhibits a semiconductor-to-metal phase transition at 68°C. VO_2 undergoes a significant change in its refractive index particularly in the NIR wavelength range as shown in Fig. 4. This makes VO_2 an important material for actively tunable optical devices with great promise for optoelectronic applications and optical gating. We are interested in modulating the SE rate of emitters at the technologically

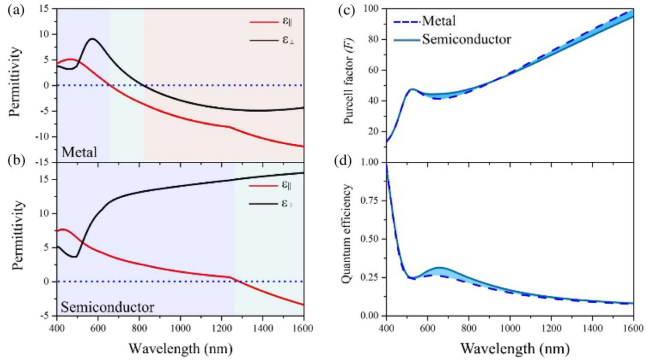

Fig. 5. Effective permittivity when VO_2 is in (a) metal phase and (b) semiconductor phase. (c) The Purcell factor and (d) QE for both phases.

important telecommunication wavelength range (1.3–1.6 μm), which can be obtained, for example, using erbium (Er) emitters.

Cueff *et al.* [21] modulated the SE rate of Er emitters utilizing VO_2 phase transition by controlling the interference between the electric and magnetic dipoles in Er ions and the light reflected from a metal–VO_2–dielectric stack. Here, we introduce an active HMM using a six-bilayer stack of TiN (20 nm) and VO_2 (40 nm). Again, TiN is used as a metal due to its lower complex permittivity compared to noble metals, which behave very closely to a perfect electric conductor in the NIR wavelength range. The optical constant of VO_2 was calculated following Kana *et al.* [22].

Figure 5(a) shows the effective parallel $\varepsilon_\parallel$ and perpendicular $\varepsilon_\perp$ permittivities of the active TiN/VO_2 HMM. For the TiN/VO_2 (metal) HMM, we observe a transition to type II HMM (green shaded region) within the $\lambda \sim 650$ nm to 815 nm beyond, which the stack behaves as a metal. On the other hand, the TiN/VO_2 (semiconductor) HMM undergoes a topological transition to a type II HMM for wavelengths $\lambda > 1290$ nm [see Fig. 5(b)]. Not surprisingly, the calculated Purcell factor F is higher for the TiN/VO_2 (metal) HMM within $\lambda \sim 550 - 850$ nm, while F is higher for the TiN/VO_2 (semiconductor) HMM for $\lambda > 1000$ nm [see Fig. 5(c)].

The acceleration of the SE rate for wavelengths preceding the topological transitions is likely due to the enhanced SE rate for epsilon-near-zero (ENZ) wavelengths due to the slow group velocity and high LDOS at ENZ wavelengths [23]. The emission of a dipole on either HMM is significantly quenched as evident in Fig. 5(d). However, for the type-I HMM transition for the TiN/VO_2 (semiconductor) HMM, the QE is noticeably higher.

Graphene is an atomically thick two-dimensional layer of carbon atoms arranged in a hexagonal lattice, which possesses unique optical, electrical, mechanical, and heating properties. The tunability of graphene's optical properties makes it ideal for active photonic and optoelectronic devices. Graphene's carrier density and conductivity can be controlled via an external gate voltage that controls the carrier concentration. In the proposed HMM, the graphene is acting as a metal when it is electrically doped [24]. The conductivity of graphene as a function of its chemical potential was determined as follows [25].

To construct an HMM in the MIR wavelength range using graphene, we chose MgF_2 as the dielectric layer as it does not

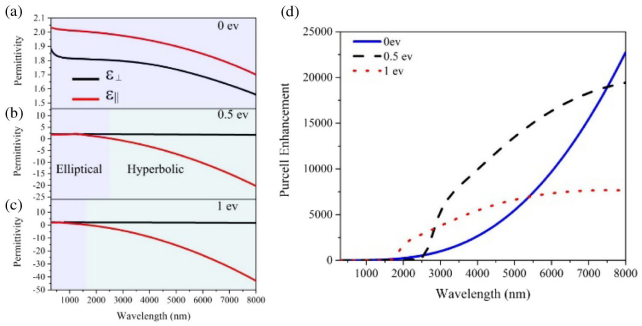

Fig. 6. Tunable spontaneous emission rate in the MIR: (a) effective parallel and perpendicular permittivity of a five-bilayer graphene/MgF_2 HMM. The hyperbolic region is shifted toward shorter wavelengths as we increase the graphene chemical potential, and graphene becomes more metallic. (b) The corresponding Purcell enhancement shows considerable increase in the Purcell enhancement at shorter wavelengths as we increase the chemical potential.

exhibit any phonon resonance in the wavelength range of interest, i.e., it has low refractive index and negligible optical losses. MgF_2 thickness (5 nm) been optimized to achieve a topological transition point at 1500 nm for 1 eV chemical potential of graphene. Without electrically doping graphene, the multilayer stack does not experience any topological transitions as graphene does not behave as a metal [see Fig. 6(a)]. However, for chemical potential values of $\mu = 0.5$ eV [Fig. 6(b)] and $\mu = 1$ eV [Fig. 6(c)], the multilayer structure effective permittivity shows type-II hyperbolic for wavelengths longer than 2500 nm and 1500 nm, respectively. Correspondingly, the calculated Purcell factor experiences a sudden increase at 2500 nm and 1500 nm, for $\mu = 0.5$ eV and $\mu = 1$ eV, respectively [Fig. 6(d)].

In conclusion, we numerically investigated tuning the SE rate of quantum emitters in the vicinity of an active HMM over the visible, NIR, and MIR wavelength ranges. The local density of states of multilayer HMMs that contains at least an optically tunable film can be modified significantly. We showed that Sb_2S_3 and VO_2 are suitable tunable materials for an active HMM in the visible and NIR wavelength ranges, respectively. The metal of choice for the visible and NIR tunable HMMs is TiN due to its low complex permittivity compared to noble metals, which accentuate the effect of tuning the optical properties of the accompanying dielectric film. In addition, we showed that a graphene/MgF_2 HMM is suitable for tunable emission rate in the MIR wavelength range. Controlling the quantum efficiency in the visible range was demonstrated and can have applications in display technologies. The proposed lithographically free platform for tuning the emission rate could be used as a basis of an all optical, or an optoelectronic modulator.

Funding. National Key Research and Development Program of China (2018YFB1107202); Strategic Priority Research Program of the Chinese Academy of Sciences (XDA22010302); Jilin Provincial Science & Technology Development Project (20180414019GH); K.C. Wong Education Foundation (GJTD-2018-08).

Acknowledgment. S. C. acknowledges his sponsorship by "CAS-TWAS President's Fellowship for international doctorate students."

Disclosures. The authors declare no conflicts of interest.

REFERENCES

1. C. L. Cortes, W. Newman, S. Molesky, and Z. Jacob, J. Opt. **14**, 063001 (2012).
2. M. Pelton, Nat. Photonics **9**, 427 (2015).
3. E. M. Purcell, H. C. Torrey, and R. V. Pound, Phys. Rev. **69**, 37 (1946).
4. C.-Y. Jin, R. Johne, M. Y. Swinkels, T. B. Hoang, L. Midolo, P. J. van Veldhoven, and A. Fiore, Nat. Nanotechnol. **9**, 886 (2014).
5. M. ElKabbash, E. Miele, A. K. Fumani, M. S. Wolf, A. Bozzola, E. Haber, T. V. Shahbazyan, J. Berezovsky, F. De Angelis, and G. Strangi, Phys. Rev. Lett. **122**, 203901 (2019).
6. F. Pagliano, Y. Cho, T. Xia, F. van Otten, R. Johne, and A. Fiore, Nat. Commun. **5**, 5786 (2014).
7. T. V. Shahbazyan, Phys. Rev. B **99**, 125143 (2019).
8. T. V. Shahbazyan, Phys. Rev. Lett. **117**, 207401 (2016).
9. Y.-J. Lu, R. Sokhoyan, W.-H. Cheng, G. Kafaie Shirmanesh, A. R. Davoyan, R. A. Pala, K. Thyagarajan, and H. A. Atwater, Nat. Commun. **8**, 1631 (2017).
10. K. J. Tielrooij, L. Orona, A. Ferrier, M. Badioli, G. Navickaite, S. Coop, S. Nanot, B. Kalinic, T. Cesca, L. Gaudreau, Q. Ma, A. Centeno, A. Pesquera, A. Zurutuza, H. de Riedmatten, P. Goldner, F. J. García de Abajo, P. Jarillo-Herrero, and F. H. L. Koppens, Nat. Phys. **11**, 281 (2015).
11. L. Lu, R. E. Simpson, and S. K. Valiyaveedu, J. Opt. **20**, 103001 (2018).
12. I. V. Iorsh, I. S. Mukhin, I. V. Shadrivov, P. A. Belov, and Y. S. Kivshar, Phys. Rev. B **87**, 075416 (2013).
13. M. A. K. Othman, C. Guclu, and F. Capolino, Opt. Express **21**, 7614 (2013).
14. Z. Cao, X. Xiang, C. Yang, Y. Zhang, Z. Peng, and L. Xuan, Liq. Cryst. **43**, 1753 (2016).
15. K. V. Sreekanth, Q. Ouyang, S. Sreejith, S. Zeng, W. Lishu, E. Ilker, W. Dong, M. ElKabbash, Y. Ting, C. T. Lim, M. Hinczewski, G. Strangi, K.-T. Yong, R. E. Simpson, and R. Singh, Adv. Opt. Mater. **7**, 1900081 (2019).
16. H. N. S. Krishnamoorthy, Y. Zhou, S. Ramanathan, E. Narimanov, and V. M. Menon, Appl. Phys. Lett. **104**, 121101 (2014).
17. W. Dong, H. Liu, J. K. Behera, L. Lu, R. J. H. Ng, K. V. Sreekanth, X. Zhou, J. K. W. Yang, and R. E. Simpson, Adv. Funct. Mater. **29**, 1806181 (2019).
18. K. V. Sreekanth, P. Mahalakshmi, S. Han, M. S. Mani Rajan, P. K. Choudhury, and R. Singh, Adv. Opt. Mater. **7**, 1900680 (2019).
19. G. V. Naik, B. Saha, J. Liu, S. M. Saber, E. A. Stach, J. M. K. Irudayaraj, T. D. Sands, V. M. Shalaev, and A. Boltasseva, Proc. Natl. Acad. Sci. USA **111**, 7546 (2014).
20. D. Lu, J. J. Kan, E. E. Fullerton, and Z. Liu, Nat. Nanotechnol. **9**, 48 (2014).
21. S. Cueff, D. Li, Y. Zhou, F. J. Wong, J. A. Kurvits, S. Ramanathan, and R. Zia, Nat. Commun. **6**, 8636 (2015).
22. J. B. K. Kana, J. M. Ndjaka, G. Vignaud, A. Gibaud, and M. Maaza, Opt. Commun. **284**, 807 (2011).
23. M. H. Javani and M. I. Stockman, Phys. Rev. Lett. **117**, 107404 (2016).
24. B. Wang, X. Zhang, F. J. García-Vidal, X. Yuan, and J. Teng, Phys. Rev. Lett. **109**, 073901 (2012).
25. J. Gosciniak and D. T. H. Tan, Sci. Rep. **3**, 1897 (2013).